Interaction of silver nanoparticles with aerobic granular sludge in textile wastewater treatment bioreactors

Bento, J.B

Abstract

The use of silver nanoparticles (Ag NPs) in textile industry has been increasing and their occurrence in wastewater is expected to rise accordingly. The antimicrobial properties of Ag NPs suggest a potential negative impact on biological wastewater treatment systems. This study assessed the impacts of 5mg L^{-1} Ag NPs on aerobic granular sludge (AGS) in sequencing batch reactors treating textile wastewater. Nuclear microscopy (NM) was applied for imaging and quantitative elemental analysis. Successful granulation was achieved after 35 days, irrespective of Ag NP presence. Although Ag NPs had induced an early AGS deterioration, in the long term they seemed to enhance AGS settling properties. Furthermore, AGS treatment performance and cell integrity were not affected by Ag NPs. A quantitative analysis of the major fractions of the extracellular polymeric substances (EPS) suggested that Ag NPs interacted with the protein fraction, which was further confirmed by NM. The Ag NPs-containing sample examination through NM also showed that < 10μm Ag NPs agglomerates were presumably distributed uniformly in the surface of both granular and floc-like structures, although in AGS it was preferentially associated with an external EPS layer. The Ag distribution in AGS demonstrated that the granule outer layers hindered the dispersion of Ag NPs into the central part. Overall, AGS showed the ability to withstand Ag NPs toxicity, but granule structural stability was negatively influenced by Ag NPs. Furthermore, the detailed NM compartmentalization of Ag NPs in sludge components provided new and relevant information concerning the pattern of Ag NPs retention.

Keywords: silver nanoparticles; aerobic granular sludge; extracellular polymeric substances; textile wastewater; sequencing batch reactor; nuclear microscopy.

1. Introduction

Textile wastewaters are rated among the most polluting of all industrial sectors, both in terms of discharged volumes and composition. The most important environmental problems arise from the high organic loads and the presence of color[1]. Nonetheless, the use of silver nanoparticles (Ag NPs) in the textile industry has been rapidly increasing and their occurrence in wastewater is expected to rise accordingly, constituting an emerging environmental concern[2,3].

Ag NPs have been incorporated into textiles to add antimicrobial functionality[4]. Ag NPs can impose toxicity to microorganisms through several mechanisms: Ag NPs can attach to cell membranes and cause changes in their permeability; small Ag NPs (<10 nm) and released Ag^{+} may enter the bacterial cells and cause cellular enzyme deactivation, membrane permeability disruption and accumulation of intracellular radicals, resulting in microbial growth inhibition, cell lysis and death[5,6]. Thus, these properties of Ag NPs suggest a potential negative impact on biological sludge in wastewater treatment.

Staged anaerobic–aerobic sequencing batch reactor (SBR) systems using the novel aerobic granular sludge (AGS) technology have been proposed as an effective alternative to the currently used flocculent activated sludge[7]. Aerobic granules are compact and dense self-aggregated microorganism clusters embedded in extracellular polymeric substances (EPS) formed under specific SBR operation conditions[8]. They have a well-defined appearance and are visible as separate entities[9]. In addition to the general advantages of the staged SBR technology, AGS systems present several unique attributes: excellent settling properties, allowing shorter settling times for good solid–liquid separation and requiring lower construction area; good biomass retention, allowing higher concentration in the SBR and consequently lower reaction time and/or reactor volume; ability to withstand toxicity and high organic loading rates [10]; aerobic and anoxic/anaerobic zones within the granules, allowing organic matter, nitrogen and phosphorus removal in the same system[11]; maintenance of stability during a storage or starvation period of weeks or months[12]. Given the particular attributes of aerobic granules, this compact technology has a great potential for the treatment of the highly variable textile wastewaters[7].

Despite the increasing reported applications of AGS for textile wastewater treatment only a few studies have been reported on the interactions of Ag NPs with AGS[5,8]. Overall, these studies have been demonstrated that Ag NPs did not cause acute toxicity to the AGS, but their chronic toxic effects are cause for great concern[5,8]. In order to better understand the causes of Ag NPs chronic toxic effects and further operate AGS systems to overcome these toxic effects it is essential to study the fate, the transformations and the toxicity mechanisms of Ag NPs. However, this information is very limited and the lack of proper techniques to trace Ag NPs in complex matrices hinders the investigation[13].

Nuclear microscopy (NM) employs high energy ion beams focused at submicron resolution to provide simultaneously elemental imaging and quantitative elemental analysis of biological material down to the parts per million (ppm) level of analytical sensitivity[14]. Furthermore, this tool only needs a simple and non-destructive sample preparation, contrarily to other techniques that have been used[13,15]. These features make NM a

promising technique to study the interactions of Ag NPS with AGS.

The objective of this study was to assess the effects of 5mg L^{-1} Ag NPs in the characteristics and performance of AGS in an anaerobic-aerobic SBR system treating synthetic textile wastewater. For that, the performance of two SBRs run in parallel, one supplied with Ag NPs and the other used as Ag NPs-free control, was evaluated in terms of COD and color removal efficiency. Additionally, this study also aimed to assess the impacts of Ag NPs on granule formation and long-term stability; on sludge mass density; on cell membrane permeability; and on the major EPS components, i.e. PN and PS. Nuclear microscopy was also applied to image elemental distribution and to perform a quantitative elemental analysis of the Ag NPs-containing sludge samples.

2. Materials and methods

2.1. Experimental system and SBR cycle operation

The experimental system was composed of two anaerobic–aerobic sequencing batch reactors (SBRs). Both SBRs were fed with a synthetic textile wastewater containing a COD:N:P mass ratio of 100:3.7:37, avoiding the occurrence of nitrification. This solution was separately added to both SBRs, as carbon feed solution (Feed - C) and nitrogen dye-containing feed solution (Feed – N). One SBR was supplied with Ag NPs (SBR1) and the other was used as Ag NPs-free control (SBR2). These SBRs were run in parallel for 271 operating days. The Ag NPs was fed to SBR1 along a 178-days operational period followed by a 60-day period during which Ag NPs were absent from the feed. After this cleaning period, Ag NPs feeding was resumed. SBR1 and SBR2 were run in 6-h cycles with a hydraulic retention time (HRT) of 12 h. Each cycle consisted of five discrete sequential phases, namely fill, reaction, with a mixed anaerobic stage followed by an aerated stage, settle, drain and idle, a quiescent period to complete the cycle time. The SBRs had a working volume of 1.5 L (height/diameter ratio of 2.5) and were fed with Feed -N and -C at the bottom with an exchange ratio of 50% and a volumetric organic loading rate (OLR) of 2.0 kg COD m^3 d^{-1}. At the end of the fill phase, SBR1 was supplied with Ag NPs at the top of the bioreactor.

2.2 Simulated textile wastewater

The Feed-C solution was prepared by diluting the carbon source stock solution (100g L^{-1}) in distilled water to a COD content of 1000 mg O_2 L^{-1} (1.15 g L^{-1} Emsize E1) and supplemented with nutrients to the following concentrations: 27.5 mg L^{-1} $CaCl_2$; 22.5 mg L^{-1} $MgSO_4 \cdot 7H_2O$; 250 μg L^{-1} $FeCl_3 \cdot 6H_2O$. The preparation of the Emsize E1 stock solution (100 g L^{-1}) was based on one set of desizing conditions provided by the manufacturer [16]. The Feed - N was prepared with phosphorus and nitrogen salts, an azo dye (AR14, Chromotrope FB, Sigma Aldrich, 50% dye content) and other micro-nutrients to the following concentrations: 2310 mg L^{-1} $Na_2HPO_4 \cdot 12H_2O$; 762 mg L^{-1} KH_2PO_4; 143 mg $L^{-1}NH_4Cl$; 40 mg L^{-1}AR14; 40 μg L^{-1} $MnSO_4 \cdot 4H_2O$, 57 μg L^{-1} H_3BO_3, 43 μg L^{-1} $ZnSO_4 \cdot 7H_2O$ and 35 μg L^{-1} $(NH_4)_6Mo_7O_{24} \cdot 4H_2O$. The dye stock solution was prepared by dissolving AR14 in distilled water to a final concentration of 5.0 g L^{-1}. The AR14 concentration at the onset of the reaction phase (after the fill phase) was 20 mg L^{-1}. The feed suspension of Ag NPs was prepared by dispersing 100 mg of Ag NPs (in the form of nanopowder, <100 nm particle size, Sigma Aldrich) in 1L milli-Q water and sonicating it (VWR, Internation bvba/sprl, Belgium) during 60 minutes at 80W. After sonication, this suspension was diluted to 1L with milli-Q water to a final concentration of 50 mg L^{-1}. The Ag NPs concentration at the onset of the reaction phase (after the fill phase) was 5 mg L^{-1}. The particle size distribution of the feed suspension of Ag NPs was determined by dynamic light scattering (DLS) (Zetasizer nanoZS, Malvern Instruments, UK). The average particle size in this solution was 155 ± 40 nm.

2.3 SBR inoculation and aerobic granulation

SBR1 and SBR2 were inoculated with activated sludge flocs (5g TSS L^{-1}) harvested from a full-scale, conventional municipal WWTP (Chelas, Lisboa, Portugal). Aerobic granulation was induced by applying progressively smaller settling times, sufficient high shear stress and a feast/famine regime. The settling times were reduced from 1 hour to 5 minutes along the first 28 days of operation. Thereafter, the settling time was maintained in 5 minutes. The required shear stress was achieved by mechanical mixing during the anaerobic phase and by aeration in the aerobic phase. The SBRs were also fed in a short feeding time (30 minutes) during the anaerobic phase, allowing to establish a long famine phase.

2.4 SBR cycle monitoring

Mixed liquor total suspended solids (MLTSS), mixed liquor volatile suspended solids (MLVSS) and pH were determined according to standard procedures[17]. Sludge volume index (SVI) was determined by measuring the volume occupied by the sludge settled from 1 L of mixed liquor after settling times of 5 and 30 min in an Imhoff cone (SVI_5 and SVI_{30}, respectively), and dividing it by the mixed liquor TSS value. Samples were collected from the two SBRs along different treatment cycles and were clarified by centrifugation (1o min at 4000 rpm) prior to dissolved COD and color analyses. Dissolved COD was determined according to standard procedures[17] and color was measured spectrophotometrically against deionized water. Absorbance spectra between 200 and 800 nm were collected from solutions of Acid Red 14 with different concentrations and a calibration curve was established using the absorbance values at the maximum absorbance wavelength in the visible region (515 nm). The concentration of dye in samples collected from SBR systems was determined in terms of color equivalents (dye-color) based on the previously established calibration curve at 515 nm, which was the only absorption peak observed in the visible region for all the collected SBR samples.

2.5 Cell Membrane permeability analysis

For membrane permeability analysis, 5mL samples were collected at the beginning of the aerated phase of one treatment cycle on operational day 258. These samples were dewatered by centrifugation at 4000 rpm for 5 min and the pellet was ressuspended in 0.85% NaCl to their original volume. This steps was repeated 2 times. In the last time, the pellet was ressuspended in 2 mL 0.85% NaCl. Then, the sludge samples were stained using the LIVE/DEAD *Bac*Light Bacterial Viability Kit (Molecular Probes, Netherlands) and were observed at magnifications of 40x, under a transmission light microscope (BA200, Motic, China) fitted with a digital camera and respective software (Moticam 1000, Motic, China).

2.6 Extracellular polymeric substances (EPS) analysis

For extracellular polymeric substances (EPS) analysis, 5 mL samples duplicates were collected along the reaction phase of one treatment cycle on operational days 243, 250, 258 and 271. These samples were dewatered by centrifugation at 4000 rpm for 10 min and stored at -80ºC until EPS extraction and analysis were performed. Before EPS extraction, the stored sludge samples, once at room temperature, were re-suspended in deionized water to their original volume. The resuspension was performed by mixing vigorously with a pipette until a homogeneous sludge suspension was obtained. The extraction of the bound EPS from sludge samples was carried out by heating the mixture suspensions to 80 °C for 30 min in a water bath. Then, the suspensions were cooled down to room temperature and centrifuged at 4000 rpm for 20 min. Prior to EPS component analysis, the supernatant was filtered through glass microfiber filter discs (Whatman, GF/C, ø 25 mm). The protein (PN) content was determined with Pierce® BCA protein assay kit using bovine serum albumin (BSA) as standard. The polysaccharide (PS) content was analyzed in accordance to the method described Dubois et al. (1956)[18] with some modifications. Briefly, 1 mL of 5% phenol (w/w) in water was added to 1 mL of sample. Then, 5 mL of concentrated sulphuric acid was added rapidly, on the liquid surface. The mixtures were allowed to react for 10 min, then were mixed and allowed to react for another 30 min at room temperature. 300 μL of each tube was pipetted to a microplate and the absorbance was measured at 490 nm. Glucose was used as standard for method calibration, in a concentration range between 0 and 500 mg L^{-1}.

2.7 X-ray microtomography analysis

Sludge samples were collected directly from the Ag NPs-fed SBR1 and control SBR2 during the aerated reaction phase of one treatment cycle on operational day 243. These samples were lyophilized (Modulyo®, Edwards, US) and the material directly mounted onto an appropriate support in a self-supported mode. Digital radiographs can be produced using an X-ray cone incident on a rotating specimen. In this study a Skyscan1172 (Brucker® USA) scanner was used. The experimental acquisition conditions included: X-ray source (voltage 59 kV, current = 167 μA, power 10W), direct irradiation without filtering with an exposure of 1000 ms/radiograph, rotation step of 0.5° (383 radiographs) and an image pixel size of 2.35 μm. The acquisition was performed by rotating the specimen over 180°. The instrument comprehends a 1.3 Megapixel camera which can reach spatial resolutions of 5 μm with a detail detectability of 2 μm. The maximum object diameter is 20 mm for standard operation and 37 mm with a camera offset. Reconstruction was performed with the NRecon (Brucker®) program with a GPUReconServer reconstruction engine. Around 1000 slices of the each sample were obtained after less than a minute and a half. 3D models and section analysis was performed with CTVox and Dataviewer free Brucker® software's. The data set after acquisition consisted of transmission X-ray images presented in Hounsfield units (HU) or attenuation coefficient units (mm^{-1}).

2.8 Nuclear Microscopy

Sludge samples were collected directly from the SBR during the aerated reaction phase of one treatment cycle on operational day 243. Aliquots of 50 μL of the sludge samples were directly deposited onto carbon conductive adhesive disks for microscopy (Agar Scientific, UK). AGS were manually detached from flocculent sludge fraction under the microscope. The prepared sludge targets were then quench-frozen in liquid nitrogen to ensure biomass integrity [19], transferred to a cryostat and allowed to dry at -25ºC. Granular structures were further encapsulated in a resin for microscopy (Tissue-Tek O.C.T. Compound). Then, it was rapidly quench-frozen in liquid nitrogen followed by sectioning in a cryostat at -25ºC. Sections of 20 μm thick were allowed to dry at -25ºC inside the cryostat. Some sections were chosen under optical microscopy and were mounted in self supported mode. The samples were examined at the proton microprobe installed at the Van de Graaf accelerator of Centro Tecnológico e Nuclear/IST (Loures, Portugal). A focused 2.0 MeV proton beam of typically 3 μm was used to scan across a selected area of interest of the sample. Data acquisition and map construction are performed with OMDAQ[20]. The spectra analysis and quantitative determination of elemental contents were carried out using the DAN32[21] computer code. The program incorporates a graphical user interface to the PIXE analysis program and a RBS simulation and fitting module. The calculation of elemental concentrations is performed using the "Q factor" charge normalization method using simultaneous PIXE and RBS analysis.

3. Results and Discussion

3.1 Effects of Ag NPs on granulation

The MLVSS content and SVI profiles obtained in both SBRs along the operational time are presented in Figure 1 and 2, respectively. Along the first 28 days of operation the settling time was gradually reduced from 1 hour to 5 minutes to promote aerobic granulation. In spite of the gradual decrease of the settling time, the biomass progressively accumulated in the mixed liquor of both SBRs along the first 35 days of operation. At this point, due to the SBR geometry limitations, AGS could not continue to accumulate in the mixed liquor, leading to a loss of AGS in the effluent. As can be seen in Figure 2, in general, the sludge initially also devolved excellent settling properties, as the SVI_5 and SVI_{30} values consistently decreased in both SBRs up to day 35, reaching 62 and 40 mL gTSS-1 in SBR1, 62.4 and 39.6 mL $gTSS^{-1}$ in SBR2, respectively. Furthermore, both reactors presented progressively converging values of SVI_5 and SVI_{30}. Therefore, it was possible to conclude that aerobic granule formation was successfully achieved during this period, irrespective the presence of Ag NPs.

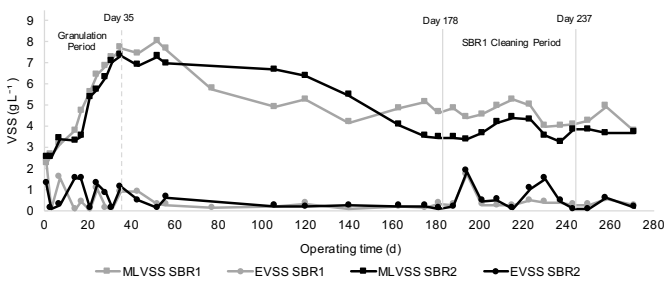

Figure 1.Volatile suspended solids profile obtained from the mixed liquor (MLVSS) and in the discharged effluent (EVSS) of the Ag NPs-fed SBR1 and of the Ag NPs-free control SBR2 along the experimental period of 271 days. The vertical dashed line indicates the end of the granulation period (Day 35), while the vertical solid lines indicate the onset (Day 178) and the end (Day 237) of the SBR1 cleaning period.

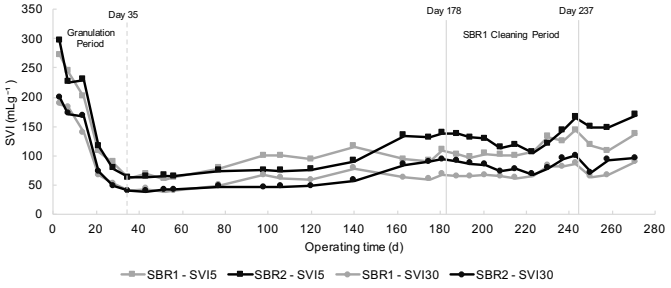

Figure 2.Volatile suspended solids profile obtained from the mixed liquor (MLVSS) and in the discharged effluent (EVSS) of the Ag NPs-fed SBR1 and of the Ag NPs-free control SBR2 along the experimental period of 271 days. The vertical dashed line indicates the end of the granulation period (Day 35), while the vertical solid lines indicate the onset (Day 178) and the end (Day 237) of the SBR1 cleaning period

3.2 Effects of Ag NPs on AGS stability

Successful aerobic granulation was attained after 35 days of SBR operation and on day 56 of the operation the Ag NPs-fed SBR1 showed a loss in its MLVSS content (Figure 1), whereas the Ag NPs-free SBR2 only exhibited a significant reduction of biomass on day 120 of the operation. As expected, the SVI profile (Figure 2) trend was consistent with that observed in the MLVSS profile, since the biomass content present in the mixed liquor is dependent of the sludge setting properties. Both the reduction of the biomass content in the mixed liquor and the loss of sludge settling capacities indicated the loss of AGS structural stability. Furthermore, the early AGS deterioration observed in the Ag NPs-fed SBR1 suggested that Ag NPs played a role on this phenomenon.

In the present study, the weakening of the AGS core due mass transfer and diffusion limitations throughout the granule structure was likely the cause of the stability loss observed in the long-term operation. The clogging of granules pores was possibly the key reason for this phenomenon. According to Lemaire et al. (2008)[22], pore clogging is related to an excess of extracellular polymeric substances (EPS) production. Recently, Corsino et al. (2016) [23]further reported that an enrichment in EPS proteins (PN), which are hydrophobic substances, can lead to an increase in granule hydrophobicity and density. As a result, granules become more compact and thick, limiting the penetration of nutrients.

The presence of Ag NPs can have contributed to the pore clogging phenomenon, thus promoting the early loss of stability observed in AGS-SBR1. Specifically, Ag NPs can have accumulated within granule pores, leading directly to their clogging, or can have either caused a shift in the composition of the microbial consortium by an increase in EPS or PN producer organisms, or the existing microbial community may have activated the metabolic pathway of EPS or PN production leading to a premature excess of EPS or an enrichment in PN. Previous research suggested that bacteria acquire higher tolerance to Ag NPs through the production of more EPS [24,25]. Thus, the increase in EPS production by AGS microorganisms was most probably a response to protect themselves from the toxic effects of the Ag NPs/Ag^+. In the study of Quan et al. (2015)[8], despite the AGS SBR with Ag NPs showing an EPS level similar to that of the Ag NPs-free control SBR after 69 days of operation, its EPS components significantly changed, with an apparent PN content increase. These authors reported that one possible explanation for the elevated production of proteins was the induction of heat shock-like proteins as a defense mechanism against high concentrations of heavy metal ions. Another possible reason for the observed EPS changes was the additional mechanical shear stress promoted by collisions between Ag NPs agglomerates and aerobic granules, as it is known that shear stress stimulates the production of EPS[26,27].

The loss of AGS stability resulted in deterioration under shear stress with the formation of small fragments with poor settling characteristics. Part of these fragments flowed out with the effluent stream and part aggregated again, forming new granules. As result, in long-term operation, the MLVSS (Figure 1) and SVI (Figure 2) profiles obtained for both SBRs reached a dynamic steady-state in which granulation and degranulation continuously occurred. Thus, the mixed liquor of both SBRs can be considered as a hybrid system of both flocculent and granular sludge. It is noted that the values of SVI and MLVSS observed during the granulation phase (first 35 days of operation) were no longer attained, suggesting that the properties of newly formed granules differ from that of the granules initially formed due to the heterogeneity of structures with less biological activity from which they had to re-develop[22].

The steady-state values of MLVSS and SVI obtained for the Ag NPs-fed SBR1 differ from those of the control SBR2. In the SVI profile, the values obtained for SBR1 tended to be lower in the long-term, suggesting that the presence of Ag NPs had a positive influence on the sludge settling capacities. Reinforcing this idea, it was also noted that during the cleaning period, the SVI_5 and SVI_{30} values gradually converged and, once the Ag NPs feeding was resumed, the values obtained for SBR1 were lower again. The SVI profile trend was consistent with the higher steady-state MLVSS values observed for the Ag NPs-fed SBR1, since the improved sludge settling capacities prevented the washout of granular sludge in the effluent stream.

These results are coherent with the effects of Ag NPs on the AGS loss of stability above discussed. Ag NPs can absorb and accumulate on the AGS, within the granule pores or on their surface, increasing directly their total density, thus improving their settling velocity. One the other hand, although a premature excess of EPS induced by the presence of Ag NPs may have induced the disintegration of the aerobic granules, EPS also contribute to a more compact and thick granular structure [23]. As a consequence, in the presence of Ag NPs, AGS can settle faster and pack more effectively in the SBR. The additional mechanical shear stress promoted by collisions between Ag NPs agglomerates and granules can not only induce the thickening of granules by enhancing EPS production, but also promote granule abrasion, resulting in smaller granules with a smoother outer surface and improved settling properties.

3.3 Effects of Ag NPs on sludge density

Microcomputerized tomography (μCT) allowed a three-dimensional (3D) reconstruction of the sludge samples from Ag NPs-fed SBR1 (Figure 3-A1) and control SBR2 (Figure 3–A2). A cross-section of each sample was also chosen (Figure 3-B1 and B2, respectively) and a representative attenuation profile was traced (Figure 3-C1 and C2, respectively).

The 3D model of the Ag NPs-exposed sludge clearly showed more frequent high attenuation regions compared to that in control. These high attenuation spots likely correspond to Ag NPs agglomerates disseminated in the biomass network, as X-rays are significantly more attenuated in Ag than in the biomaterial light element matrix. This can also be observed in more detail in the selected attenuation profiles. The attenuation profile of the Ag

NPs exposed sludge sample showed sharp and well-defined peaks corresponding to particle features in the cross-section, likely Ag NPs agglomerates. This pattern contrasted with the irregular and less prominent peaks of the attenuation profile obtained for the control sample, where the relationship between attenuation changes and particles are not so clear.

The different profiles of X-ray attenuation observed in the μCT analysis of the biomaterials can be interpreted as differences in density of the material due to the presence of Ag NPs, as the attenuation is proportional to the atomic density [28]. Taking this into account, the differences in attenuation observed permitted to conclude that the Ag NPs accumulated in sludge can effectively contribute to an increase in sample mass density, which is in line with previous results as discussed in section 3.2.

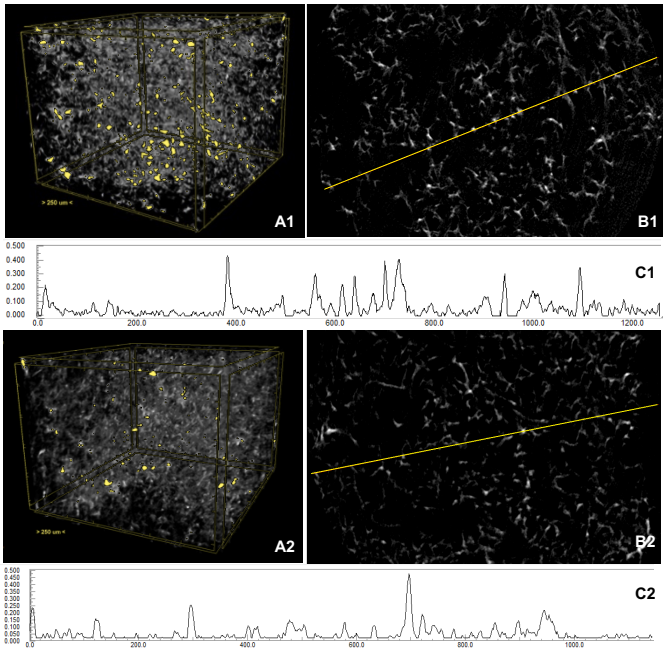

Figure 3. μCT analysis. A - 3D model of sludge sample of the SBR1 (A1) and control SBR2 (A2). Attenuation is represented by a grey scale: high attenuation – light grey, to low attenuation – dark grey. The high values of X-ray attenuation are highlighted with yellow color. B –Selected cross-section of sludge sample of the SBR1 (B1) and control SBR2 (B2). Attenuation gradient is also represented by a grey scale: high attenuation – dark grey, to low attenuation – light grey. The yellow row represents the attenuation profile present in C1 and C2. Attenuation units (y axis) are arbitrary, distance units (x axis) are in μm.

3.4 Effects of Ag NPs on SBR treatment performance

3.4.1 COD removal

The carbon load removal performance of the SBRs was evaluated through measurements of residual soluble COD levels along the experimental period. The overall residual COD values registered along the reported experimental time are represented in Figure 4. The initial high residual COD levels attained in both SBRs were probably due to the change in the nature of the main carbon substrate, from domestic wastewater to a synthetic textile wastewater with hydrolyzed hydroxypropyl starch as the carbon source. However, the sludge in both SBRs rapidly adapted to the new carbon source, reaching stable COD removal levels within the 80 to 90% range after 17 days of operation. In the Ag NPs-fed SBR1, the COD removal yield decreased on day 77, probably due to the considerable loss of mixed liquor biomass on that day (Figure 1). After that day, both SBRs maintained stable COD removal yields during the whole experimental period, irrespective of the presence of Ag NPs. Also, Quan et al. (2015) showed that Ag NP-fed reactors maintained a high COD removal similar to the Ag NPs-free control reactor throughout the whole operational period. Nonetheless, these authors suggested that probably an influent COD of 1000 mg O_2 L^{-1} was not sufficient to observe the influence of Ag NPs exposure in COD removal.

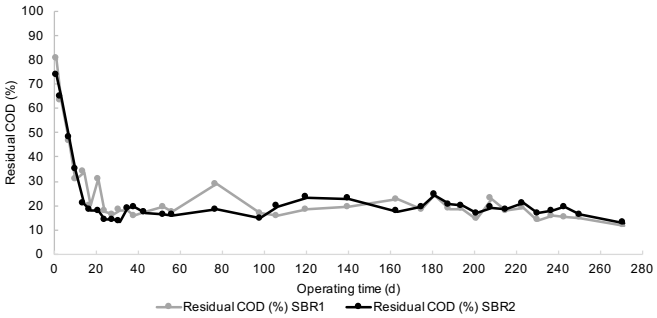

Figure 4. Overall residual COD yields in the Ag NPs-fed SBR1 and the Ag NPs-free control SBR2 along the experimental time of 271 days.

The residual COD profiles for SBR1 and SBR2 along the reaction phase of one treatment cycle selected as example (day 56) are shown in Figure 5. The COD removal profiles of SBR1 and SBR2 were similar, indicating that the presence of Ag NPs with a concentration of 5mg L^{-1} at the onset of the reaction phase did not have a significant influence on the COD removal capacity of the aerobic granules. Similar behavior was observed for the remaining treatment cycles.

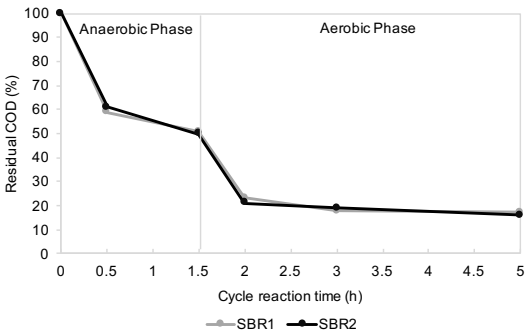

Figure 5. Residual COD profiles along the 5-h reaction phase of a typical SBR cycle (day 56) in the presence (SBR1) and absence (SBR2) of Ag NPs. Similar profiles were observed for the remaining treatment cycles. The vertical line indicates the onset of aeration.

3.4.2 Color Removal

The color removal performance of the SBRs was assessed through measurements of residual color levels along the experimental period. The overall residual color values registered along the reported experimental time are represented in Figure 6. The biomass rapidly adapted to the synthetic textile wastewater containing the azo dye AR14 since color removal levels higher than 80% were attained after 3 days of operation in both SBRs. Similarly to COD, the color removal yield decreased on day 17, probably due to the considerable loss of biomass in the effluent on that day (Figure 1). As the biomass accumulated again in the both SBRs, color removal yield was also gradually recovered. After the first 31 days, the color removal levels of SBR1 and SBR2 were similar along the reported experimental time, indicating that the presence of Ag NPs with a concentration of 5mg L^{-1} at the onset of the reaction phase did not have a significant influence on the biodecolorization process of the azo dye AR14 by AGS.

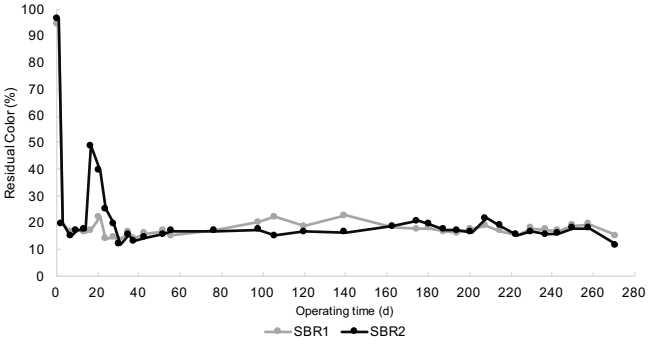

Figure 6. Overall residual color yields in the Ag NPs-fed SBR1 and the Ag NPs-free control SBR2 along the experimental time of 271 days.

Residual color profiles for SBR1 and SBR2 along the reaction phase of one SBR cycle selected as example (day 120) are shown Figure 7. As expected, the color removal occurred almost solely in the anaerobic reaction phase. Both SBRs showed similar residual color profiles along the cycle reaction time, suggesting that the exposure to Ag NPs did not have a significant influence on the anaerobic biodecolorization process. Similar behavior was observed for the remaining treatment cycles.

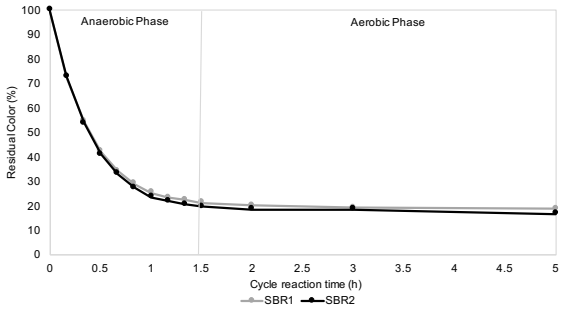

Figure 7. Residual color profiles along the 5-h reaction phase of a typical SBR cycle (day 120) in the Ag NPs- fed SBR1 and the Ag NPs-free control SBR2. Similar profiles were observed for the remaining treatment cycles. The vertical line indicates the onset of aeration.

Therefore, in the present system both COD and color removal yields and profiles of the Ag NPs-fed SBR1 and the Ag NPs-free control SBR2 showed to be similar along the reported experimental time, suggesting that the presence of Ag NPs did not have a significant influence in the SBR treatment performance.

3.5 Effects of Ag NPs on cell membrane permeability

Membrane permeability and sludge cell integrity were assessed using a mixture of SYTO 9 green-fluorescent nucleic acid stain and the red-fluorescent nucleic acid stain, propidium iodide (PI). These stains differ both in their spectral characteristics and in their ability to penetrate healthy bacterial cells. When used alone, the SYTO 9 stain generally labels all bacteria in a population – those with intact membranes and those with damaged membranes. In contrast, PI penetrates only bacteria with damaged membranes, causing a reduction in the SYTO 9 stain fluorescence when both dyes are present. Thus, comparing the stained cells present in sludge samples collected from the Ag NPs-fed SBR1 and the control SBR2 it was possible to infer the influence of Ag NPs on membrane permeability of the exposed sludge cells.

As can be depicted in Figure 8 –A1 and –A2, the examined sludge consisted of AGS presenting a structure with a regular, smooth and spherical shape with and a well-defined outer surface, surrounded by flocculent sludge with a loose, fluffy and irregular structure. The presence of Ag NPs could be further identified by a darker color in the Ag NPs-fed SBR1 sludge, mainly associated to the flocculent structures. Both sludge fractions exposed to Ag NPs showed no significant difference compared to control in terms of dead cells (Figure 8 (B1 –B2)) and total cells (Figure 8 (C1–C2)), indicating that the cell membranes were not damaged in the presence of Ag NPs.

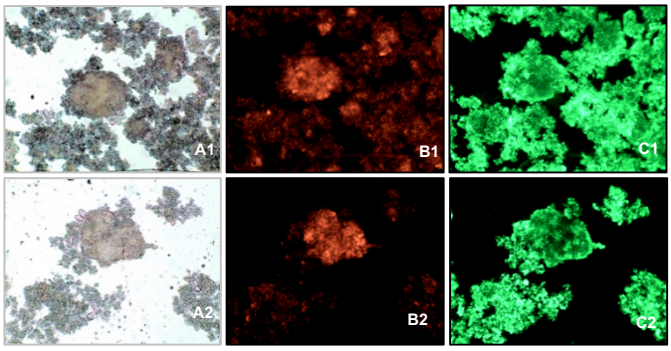

Figure 8. Ag NPs influence on cell membrane permeability inferred from LIVE/DEAD assays. Optical microscopy images of sludge samples from the Ag NPs-fed SBR1 (A1, B1 and C1) and the control SBR2 (A2, B2 and C2) without stain (A1 and A2), stained with propidium iodide (B1 and B2) and SYTO 9 (C1 and C2). The SYTO 9 stain labels all bacteria in a population (total cells). PI penetrates only bacteria with damaged membranes (dead cells).

3.7 Effects of Ag NPs on extracellular polymeric substances (EPS)

EPS was extracted from samples of the Ag NPs-fed SBR1 and from the Ag NPs-free control SBR2 mixed liquor along the reaction phase of different SBR cycles and their major constituents, i.e. proteins (PN) and polysaccharides (PS), were analyzed.

Figure 9 shows the mean PS profile obtained along the reaction phase of the studied AGS-SBR treatment cycles and a representative example of the residual COD profile (day 56) for the SBR1 and the control SBR2. As expected, it was observed an increase of PS content in the first 0.5h, as easily biodegradable COD was removed from the mixed liquor. Subsequently, a decrease in the PS content occurred during the starvation phase. It was also observed that the biodegradable EPS produced in the feast phase was consumed during the subsequent famine phase. Similar PS behavior was reported by others authors[29,30]. Although there was a small difference between the average PS profile in the anaerobic phase of SBR1 and SBR2, the PS content values and their trend did not differ significantly. Therefore, this indicates that the presence of Ag NPs did not affect the dynamic change of PS along the reaction phase.

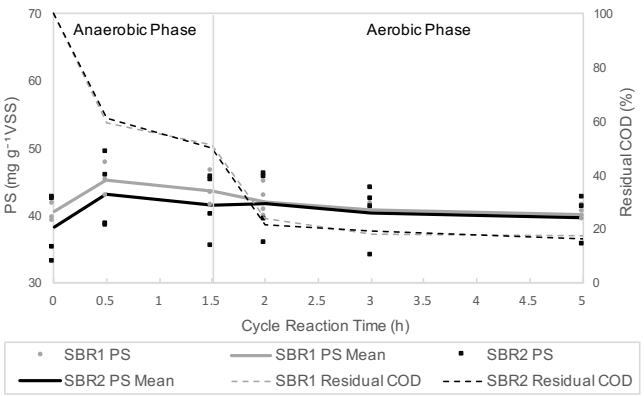

Figure 9. Average PS profile obtained along the reaction phase of the studied treatment cycles and a typical example of the residual COD profile (day 56) for the SBR1 and the control SBR2. The vertical line indicates the onset of aeration.

The average PN profile obtained along the reaction phase of the studied treatment cycles and a representative example of the

pH profile (day 243) for the SBR1 and the control SBR2 are shown in Figure 10. It was expected an increase in PN content, as COD was removed from the mixed liquor. Instead, a decrease of the PN content was observed during the anaerobic phase, similarly to the behavior detected in the pH profile. Although the phosphate buffer included in the synthetic textile wastewater was sufficient to maintain the pH in the range of 6.3 to 6.8, there is slight acidification was observed during the anaerobic phase. After the start of aeration, this trend was reversed and the PN profile acquired higher values. EPS can be subdivided into bound EPS and soluble EPS. In this comparative study, it was only analyzed the bound-EPS fraction and it was considered as representative of the EPS present in the sludge samples. Nonetheless, whenever the pH of the medium moves away from the isoelectric point of a protein, its solubility increases. Thus, it is possible that the reduction detected in the PN content of the bound EPS was related to the slight acidification of the medium in the anaerobic phase, as some proteins might have solubilized.

Similar pH profiles were achieved for SBR1 and control SBR2, suggesting that the presence of Ag NPs did not affect the pH profile. On the contrary, considerably higher PN levels were obtained for the control SBR2 than for the Ag NPs-fed SBR1. This can be explained by limitations of the PN quantification method. The bicinchoninic acid (BCA) protein assay combines the reduction of Cu^{2+} to Cu^{+} by protein in an alkaline medium with the colorimetric detection of the Cu^{+} by BCA. The color development results from the reaction of two molecules of BCA with one Cu^{+}, forming the complex 2(BCA)–Cu. Nonetheless, this reaction is strongly influenced by four amino acid residues, including cysteines (Cys). Specifically, in the presence of proteins enriched in Cys, the Cu^{+} can form the complex BCA–Cu^{+}–Cys and Cys–Cu^{+}–Cys, in addition to the 2(BCA)–Cu complex, producing an overestimated result [31]. Therefore, as Ag NPs/Ag^{+} has a strong affinity with the thiol (–SH) group of Cys present in EPS proteins[32,33], it is possible that Ag NPs/Ag^{+} hinder the formation of these complexes. This means that the PN levels observed for the control SBR2 could have been overestimated by limitations of the method. Although this result has prevented the study of the behavior of PN along the reaction phase of the studied treatment cycles, it permitted to conclude that the Ag NPs/Ag^{+} interacted with this EPS component, suggesting that PN possibly take part in the reported protective role of EPS to the inner microorganisms against Ag NPs/Ag^{+} in this system.

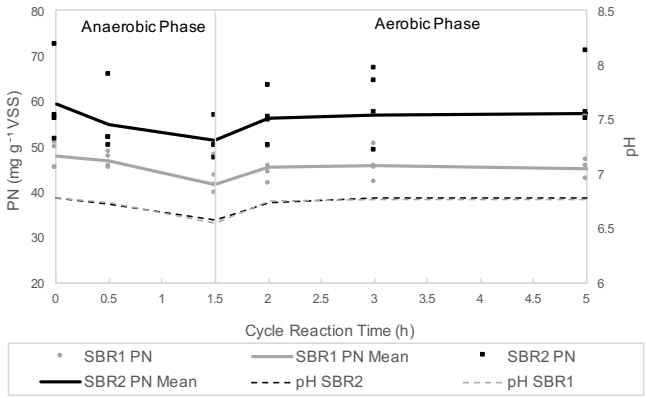

Figure 10. Average PN profile obtained along the reaction phase of the studied treatment cycles and a typical example of the pH profile (day 243) for the SBR1 and the control SBR2. The vertical line indicates the onset of aeration.

3.8 Sludge characterization and Ag NPs distribution

Nuclear microscopy was applied to image elemental distribution, as well as to perform a quantitative elemental analysis of the Ag NPs-containing sludge samples. Both flocculent and granular sludge were present in the SBR samples collected for nuclear microscopy examination. The sample preparation methodology adopted aimed the separation of these two sludge fractions and ensure that elemental contents and Ag NPs burdens in AGS and flocculent sludge could be properly analyzed and estimated. As can be observed in Figure 11–A, the flocculent sludge was separated from the AGS, although some remaining flocculent sludge involving the granule could not be completely detached. In AGS, it was also possible to distinguish an external gel-like layer surrounding the spheroid structure of the granule. Similar gel-like layers, mainly constituted by loosely bound EPS (LB-EPS), have previously been reported by Sheng et al. (2010)[34].

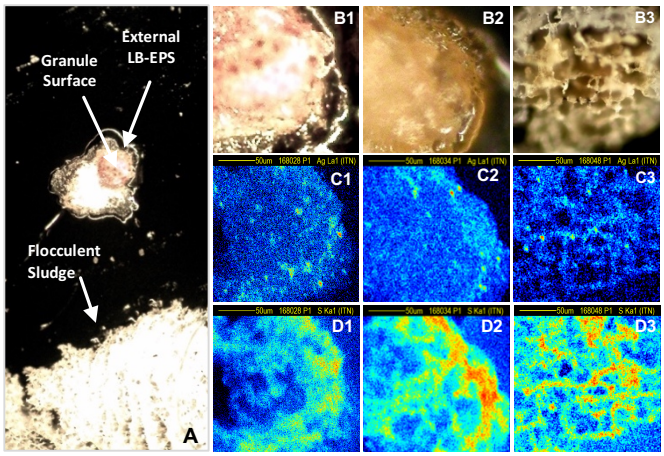

Figure 11. Sludge characterization. Optical micrographs of AGS and flocculent sludge (100x magnification). Dehydrated sample showing a manually isolated AGS granule surrounded by external EPS and flocculent sludge (A); details of AGS surface (B1–B2) and dehydrated flocs (B3). Nuclear microscopy elemental distribution maps of Ag (C1-C3) and S (D1-D3) of AGS and flocculent sludge depicted above. Content gradient is represented by a color dynamic scale: high content – red, low content – blue. Sludge samples were collected directly from the Ag NPs-fed SBR1 during the aerated reaction phase of one treatment cycle on operational day 243

The nuclear microscopy examination of the sludge showed that the presence of Ag NPs could be easily visualized in both AGS structures and flocculent sludge. Ag NPs typically clustered in agglomerates presenting a dimension < 10 μm, which were invariably distributed throughout the AGS and flocculent sludge, but were not observed in the surrounding medium. The images of Ag distribution showed an apparent predominance of Ag NPs agglomerates on the AGS regions coated with the gelatinous film (Figure 11 C1–C2), while Ag deposits on the exposed surface regions of the granules seem to be less important. This result is consistent with the reported affinity of EPS for metals[35,36]. Specifically, the loosely network of LB-EPS may facilitate the physical retention of Ag NPs and promote the capture of Ag NPs in its structure[36]. However, because of the sample preparation methodology adopted part of the dispersible EPS layer was dragged to the edges of the spheroid structure. This means that in the native sludge most probably this layer is distributed uniformly on the granule surface, as well as the Ag associated to it. This also imply that the external EPS layer may prevent Ag NPs to interact with the inner layer of the granules. In turn, the images of Ag distribution in flocculent sludge (Figure 11 –C3) showed Ag NPs

clusters uniformly distributed along the characteristic laminar like structure.

Furthermore, as can be easily visualized in PIXE maps presented in Figure 11 C (1–3) and D (1–3), the S distribution in both sludge structures seemed to follow the Ag distribution. The S content is related with protein content, as proteins contain abundant thiol (–SH) groups. Therefore, this pattern suggested the Ag NPs/Ag^{+} interact with extracellular proteins present in EPS matrix, which is line with the interaction previously discussed in EPS protein quantification.

Ag NPs clusters, which can be visualized in the PIXE Ag distribution maps, may be embedded in both sludge structures. This means that RBS spectra analysis in these regions often has to account for Ag at a certain depth below the surface and both matrix estimation and depth distribution of Ag are therefore not straightforward. In addition, the depth of biomaterial (either AGS or flocculent sludge) that could be probed with 2.0 MeV protons was approximately 4-6 μm, which definitely limited the capability of assessing Ag profiles in these structures. Taking these limitations and derived uncertainties into account and for comparison purposes, the Ag quantification in the surface of AGS and flocculent sludge was carried out. The amount of Ag, whether associated to flocculent sludge or AGS surface, did not significantly differ (Figure 12). This suggests that Ag NPs remained attached or entrapped in the surface of both sludge structures in a similar manner. Nonetheless, this does not mean that there were no differences in the inner layers of the sludge components.

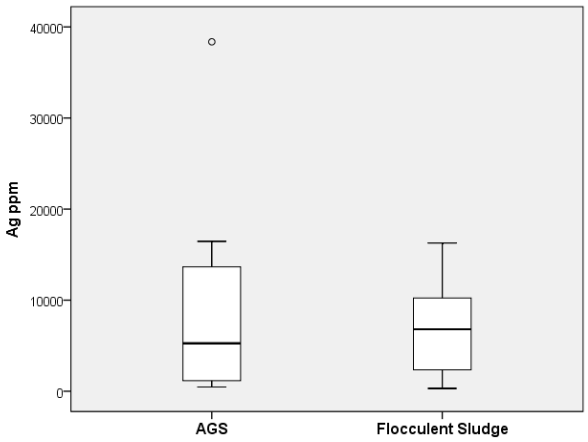

Figure 12. Box plot of the Ag concentrations in AgNPs clusters identified on the surface of AGS and flocculent sludge. The box represents the 25% and 75% interquartiles (IQ) and the dividing horizontal line indicates the median; whiskers indicate the maximum and minimum values.

The elements present in AGS are also present in flocculent sludge (Table S1). However, the quantitative approach showed a higher S content in flocculent sludge (Figure 13), whereas P, K, and Ca were mainly associated to the AGS. No significant variations in the concentrations of Cl, Mn and Zn were found in the sludge components.

The higher S content of flocculent sludge suggested a higher protein content, according to the relation previously mentioned. In fact, the flocculent sludge due to their large specific surface area with a loose structure can favor the contact between Ag NPs and cells. Thus, cells as response against the toxic effects of the Ag NPs/Ag+ can have enhanced the EPS production [24,25], presumably in the form of proteins [8]. On the other hand, the presence of high contents of P, K and Ca in granule structures is consistent with their higher cellular density [8].

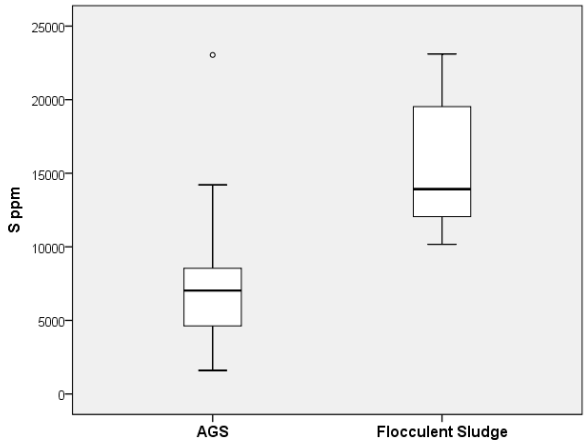

Figure 13. Box plot of the S concentrations in AGS and flocculent sludge. The box represents the 25% and 75% interquartiles (IQ) and the dividing horizontal line indicates the median; whiskers indicate the maximum and minimum values.

To explore the Ag distribution in AGS, sections of these spheroid structures were examined (Figure 14). In AGS sections an evident predominance of Ag NPs agglomerates were associated to the outer layers of the spheroid structures (Figure 14 –B1 and B2). The quantitative approach also confirmed the significantly higher Ag concentration present in the outer layer of the granule (Figure 14 –C). These results suggested that the outer layers of AGS hinder the dispersion of Ag NPs into the central part of the granule, which is in agreement with the results obtained in the granule surface analysis, as discussed above. Therefore, the retention of Ag NPS on the granule surface layers may protect the microbial communities present in the inner layers against Ag NPs/Ag^{+} toxicity. These results are in line with that reported by Quan et al. (2015)[8]. These authors suggested that the special physical structure of AGS in which microbes aggregate tightly and are encapsulated by dense layers of EPS allowed the microbial community to remain stable after long-term exposure (69 days) to 5 and 50 mg/L of Ag NPs.

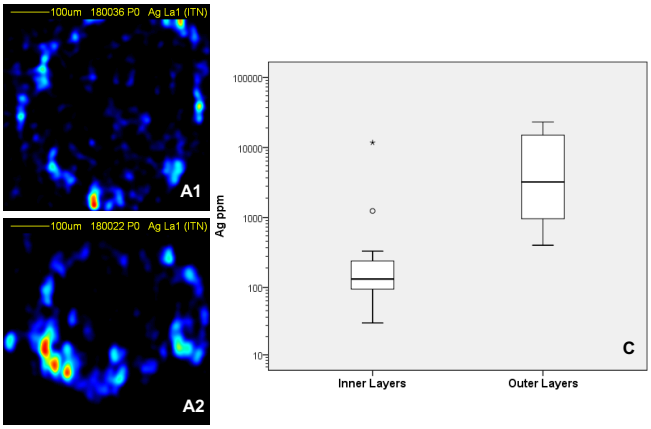

Figure 14. Ag distribution in granule sections. PIXE maps of Ag distribution (A1–A2). The content gradient is represented by a color dynamic scale: high content – red, low content – blue. B – Box plot of the logarithm of Ag concentration in Ag NPs clusters identified on the inner and outer layer of AGS. The box represents the 25% and 75% interquartiles (IQ) and the dividing horizontal line indicates the median; whiskers indicate the maximum and minimum values.

4. Conclusions

The current study represents one of the first reports assessing the effects of silver nanoparticles on the characteristics and

performance of AGS during the treatment of synthetic textile wastewater in an anaerobic-aerobic SBR system, including the granulation step. Successful granule formation was achieved after 35 days of operation, irrespective of the presence of Ag NPs. Although the exposure to Ag NPs had induced an early deterioration of the granules, in the long term Ag NPs seemed to have a positive influence on their settling properties.

The accumulation of Ag NPs within the granule pores and on their surface, a premature excess of EPS production or an enrichment in the protein fraction of EPS induced by Ag NPs, as well as the additional mechanical shear stress promoted by collisions between Ag NPs agglomerates and the granules, seemed to be the main mechanisms involved in both early AGS loss of stability and improved sludge settling capacities. Furthermore, the presence of Ag NPs apparently did not influence neither SBR treatment performance nor cell membrane integrity in the present system. The quantitative analysis of the EPS major fractions suggested that Ag NPs interact with the protein fraction, which was further confirmed by nuclear microscopy. The examination of Ag NPs-containing samples through nuclear microscopy also showed that < 10μm Ag NPs agglomerates were presumably distributed uniformly in the surface of both granular and floc-like structures, although in AGS they were preferentially associated to an external gel-like EPS layer. A quantitative nuclear microscopy approach revealed that the amount of Ag, whether associated to flocculent sludge or AGS surface, did not significantly differ. This analysis also evidenced a higher protein content for flocculent sludge, whereas granule structures appeared to have a higher cellular density. The Ag distribution in cross sectioned AGS samples demonstrated that the outer layers of the granules greatly hindered the dispersion of Ag NPs into the central part, which may have protected the microbial communities present in the inner layers against Ag NPs/Ag^+ toxicity.

This study demonstrated that AGS has the ability to withstand Ag NPs/Ag^+ toxicity, since neither SBR treatment performance nor cell membrane integrity were affected under the conditions tested. Nonetheless, the Ag NPs seemed to have negatively influenced the structural stability of AGS, which is one of the most serious barriers to full scale applications of AGS technology. Furthermore, this study provided various evidences that Ag NPs interacted with extracellular proteins present in the EPS matrix. As such, studies should be performed to better evaluate the impact of Ag NPs on this EPS component and further operate AGS systems to overcome the observed detrimental effects. The use of nuclear microscopy allowed the detailed compartmentalization of Ag NPs in sludge sample components, providing new and relevant information concerning the pattern of Ag NPs retention. Thus, the reported results also highlighted the potential application of nuclear microscopy for characterizing the fate of Ag NPs in wastewater treatment systems based in AGS technology.

5. References

1. dos Santos, A. B., Cervantes, F. J. & van Lier, J. B. Review paper on current technologies for decolourisation of textile wastewaters: Perspectives for anaerobic biotechnology. *Bioresour. Technol.* **98,** 2369–2385 (2007).
2. Som, C., Wick, P., Krug, H. & Nowack, B. Environmental and health effects of nanomaterials in nanotextiles and fa??ade coatings. *Environ. Int.* **37,** 1131–1142 (2011).
3. Windler, L., Height, M. & Nowack, B. Comparative evaluation of antimicrobials for textile applications. *Environ. Int.* **53,** 62–73 (2013).
4. Radetić, M. Functionalization of textile materials with silver nanoparticles. *J. Mater. Sci.* **48,** 95–107 (2013).
5. Gu, L., Li, Q., Quan, X., Cen, Y. & Jiang, X. Comparison of nanosilver removal by flocculent and granular sludge and short- and long-term inhibition impacts. *Water Res.* **58,** 62–70 (2014).
6. Liang, Z., Das, A. & Hu, Z. Bacterial response to a shock load of nanosilver in an activated sludge treatment system. *Water Res.* **44,** 5432–5438 (2010).
7. Lourenço, N. D. *et al.* Comparing aerobic granular sludge and flocculent sequencing batch reactor technologies for textile wastewater treatment. *Biochem. Eng. J.* **104,** 57–63 (2015).
8. Quan, X., Cen, Y., Lu, F., Gu, L. & Ma, J. Response of aerobic granular sludge to the long-term presence to nanosilver in sequencing batch reactors: Reactor performance, sludge property, microbial activity and community. *Sci. Total Environ.* **506–507,** 226–233 (2015).
9. Liu, Y. & Tay, J.-H. State of the art of biogranulation technology for wastewater treatment. *Biotechnol. Adv.* **22,** 533–563 (2004).
10. Adav, S. S., Lee, D., Show, K. & Tay, J. Aerobic granular sludge : Recent advances. *Biotechnol. Adv.* **26,** 411–423 (2008).
11. Pronk, M. *et al.* Full scale performance of the aerobic granular sludge process for sewage treatment. *Water Res.* **84,** 207–217 (2015).
12. Gao, D., Liu, L., Liang, H. & Wu, W.-M. Aerobic granular sludge: characterization, mechanism of granulation and application to wastewater treatment. *Crit. Rev. Biotechnol.* **31,** 137–52 (2011).
13. Liu, J., Yu, S., Yin, Y. & Chao, J. Methods for separation, identification, characterization and quantification of silver nanoparticles. *TrAC Trends Anal. Chem.* **33,** 95–106 (2012).
14. Mulware, S. J. The Review of Nuclear Microscopy Techniques : An Approach for Nondestructive Trace Elemental Analysis and Mapping of. **2015,** (2015).
15. Pinheiro, T., Ynsa, M. D. & Alves, L. C. in *Modern Research and Educational Topics in Microscopy* 237–244 (2007).
16. Lourenço, N. D., Novais, J. M. & Pinheiro, H. M. Reactive textile dye colour removal in a sequencing batch reactor. *Water Sci. Technol.* **42,** 321–328 (2000).
17. Eaton, A. D., Clesceri, L. S. & Greenberg, A. E. in *American Public Health Association* (1995).
18. Dubois, M., Gilles, K. a., Hamilton, J. K., Rebers, P. a. & Smith, F. Colorimetric method for determination of sugars and related substances. *Anal. Chem.* **28,** 350–356 (1956).
19. Pinheiro, T. *et al.* The influence of corneocyte structure on the interpretation of permeation profiles of nanoparticles across skin. *Nucl. Instruments Methods Phys. Res. Sect. B Beam Interact. with Mater. Atoms* **260,**

119–123 (2007).

20. Grime, G. W. & Dawson, M. Recent developments in data acquisition and processing on the Oxford scanning proton microprobe. *Nucl. Instruments Methods Phys. Res. Sect. B Beam Interact. with Mater. Atoms* **104,** 107–113 (1995).

21. Grime, G. W. Dan32 : Recent Developments In The Windows Interface To GUPIX. 8–10 (2004).

22. Lemaire, R., Webb, R. I. & Yuan, Z. Micro-scale observations of the structure of aerobic microbial granules used for the treatment of nutrient-rich industrial wastewater. *ISME J.* **2,** 528–541 (2008).

23. Corsino, S. F., Capodici, M., Torregrossa, M. & Viviani, G. Fate of aerobic granular sludge in the long-term: The role of EPSs on the clogging of granular sludge porosity. *J. Environ. Manage.* **183,** 541–550 (2016).

24. Sheng, Z. & Liu, Y. Effects of silver nanoparticles on wastewater biofilms. *Water Res.* **45,** 6039–6050 (2011).

25. Zhang, C., Liang, Z. & Hu, Z. Bacterial response to a continuous long-term exposure of silver nanoparticles at sub-ppm silver concentrations in a membrane bioreactor activated sludge system. *Water Res.* **50,** 350–358 (2014).

26. Adav, S. S., Lee, D. J. & Lai, J. Y. Effects of aeration intensity on formation of phenol-fed aerobic granules and extracellular polymeric substances. *Appl. Microbiol. Biotechnol.* **77,** 175–182 (2007).

27. Zhu, L., Dai, X., Lv, M. & Xu, X. Correlation analysis of major control factors for the formation and stabilization of aerobic granule. *Environ. Sci. Pollut. Res.* **20,** 3165–3175 (2013).

28. Rajczakowska, M., Stefaniuk, D. & Łydżba, D. Microstructure Characterization by Means of X-ray Micro-CT and Nanoindentation Measurements. *Stud. Geotech. Mech.* **37,** (2015).

29. Wang, Z., Liu, L., Yao, J. & Cai, W. Effects of extracellular polymeric substances on aerobic granulation in sequencing batch reactors. *Chemosphere* **63,** 1728–1735 (2006).

30. Deng, S., Wang, L. & Su, H. Role and influence of extracellular polymeric substances on the preparation of aerobic granular sludge. *J. Environ. Manage.* **173,** 49–54 (2016).

31. Huang, T., Long, M. & Huo, B. Competitive binding to cuprous ions of protein and BCA in the bicinchoninic acid protein assay. *Open Biomed. Eng. J.* **4,** 271–278 (2010).

32. Levard, C., Hotze, E. M., Lowry, G. V. & Brown, G. E. Environmental transformations of silver nanoparticles: Impact on stability and toxicity. *Environ. Sci. Technol.* **46,** 6900–6914 (2012).

33. Behra, R. *et al.* Bioavailability of silver nanoparticles and ions: from a chemical and biochemical perspective. *J R Soc Interface* **10,** 15 (2013).

34. Sheng, G.-P., Yu, H.-Q. & Li, X.-Y. Extracellular polymeric substances (EPS) of microbial aggregates in biological wastewater treatment systems: A review. *Biotechnol. Adv.* **28,** 882–894 (2010).

35. Kang, F., Alvarez, P. J. J. & Zhu, D. Microbial Extracellular Polymeric Substances Reduce Ag + to Silver Nanoparticles and Antagonize Bactericidal Activity Microbial Extracellular Polymeric Substances Reduce Ag + to Silver Nanoparticles and. *Environ. Sci. Technol.* **48,** 316–322 (2014).

36. Geyik, A. G. & Çeçen, F. Exposure of activated sludge to nanosilver and silver ion: Inhibitory effects and binding to the fractions of extracellular polymeric substances. *Bioresour. Technol.* **211,** 691–697 (2016).

Supplementary Material

Table 1. Elemental concentrations present in aerobic granular sludge (AGS) and Flocculent Sludge (mg/kg dry weight). Data summarized as median (IQ50%) and interquartiles 25% (IQ 25%) and 75% (IQ 75%). Significant differences, $p<0.05$, for Mann-Whitney non-parametric test are also indicated (*).

Elements (mg/kg dry weight)	AGS			Flocculent Sludge		
	IQ 25%	IQ 50%	IQ 75%	IQ 25%	IQ 50%	IQ 75%
Ag	1015	5262	15974	1841	6802	10918
S	4421	7028	8947	11960	13922	20078*
P	20173	39715	77079	16076	18659	22351*
Cl	9834	33227	42635	9998	12401	15005
K	24738	37723	61847	22356	26871	34741 *
Ca	3991	4917	13085	2884	3705	4696 *
Mn	13	18	38	10	23	27
Zn	31	44	109	34	48	87